The American Journal of Pathology, Vol. 183, No. 3, September 2013

The American Journal of
PATHOLOGY
ajp.amjpathol.org

BIOMARKERS, GENOMICS, PROTEOMICS, AND GENE REGULATION

Toward a Molecular Pathologic Classification of Urothelial Carcinoma

Gottfrid Sjödahl,* Kristina Lövgren,* Martin Lauss,* Oliver Patschan,† Sigurdur Gudjonsson,† Gunilla Chebil,* Mattias Aine,* Pontus Eriksson,* Wiking Månsson,† David Lindgren,‡ Mårten Fernö,* Fredrik Liedberg,† and Mattias Höglund*

From the Department of Clinical Sciences, Divisions of Oncology and Urology,† Skåne University Hospital, Lund University, Lund; and the Center for Molecular Pathology,‡ Department of Laboratory Medicine, Skåne University Hospital, Lund University, Malmö, Sweden*

Accepted for publication
May 7, 2013.

Address correspondence to Mattias Höglund, Ph.D., Department of Oncology/ Oncogenomics Branch, Clinical Sciences, Skåne University Hospital, Lund University, S-221 85 Lund, Sweden. E-mail: mattias.hoglund@med.lu.se.

We recently defined molecular subtypes of urothelial carcinomas according to whole genome gene expression. Herein we describe molecular pathologic characterization of the subtypes using 20 genes and IHC of 237 tumors. In addition to differences in expression levels, the subtypes show important differences in stratification of protein expression. The selected genes included biological features central to bladder cancer biology, eg, cell cycle activity, cellular architecture, cell-cell interactions, and key receptor tyrosine kinases. We show that the urobasal (Uro) A subtype shares features with normal urothelium such as keratin 5 (KRT5), P-cadherin (P-Cad), and epidermal growth factor receptor (EGFR) expression confined to basal cells, and cell cycle activity (CCNB1) restricted to the tumor-stroma interface. In contrast, the squamous cell cancer—like (SCCL) subtype uniformly expresses KRT5, P-Cad, EGFR, KRT14, and cell cycle genes throughout the tumor parenchyma. The genomically unstable subtype shows proliferation throughout the tumor parenchyma and high ERBB2 and E-Cad expression but absence of KRT5, P-Cad, and EGFR expression. UroB tumors demonstrate features shared by both UroA and SCCL subtypes. A major transition in tumor progression seems to be loss of dependency of stromal interaction for proliferation. We present a simple IHC/histology-based classifier that is easy to implement as a standard pathologic evaluation to differentiate the three major subtypes: urobasal, genomically unstable, and SCCL. These three major subtypes exhibit important prognostic differences. *(Am J Pathol 2013, 183: 681—691; http://dx.doi.org/10.1016/j.ajpath.2013.05.013)*

Assessment of urothelial carcinoma for clinical intervention is determined using standard pathologic variables. For example, the European Organisation for Research and Treatment of Cancer risk tables include tumor grade, tumor stage, and presence or absence of carcinoma *in situ*, complemented by information on previous recurrence rate, tumor diameter, and number of tumors. Although these tables are efficient in controlled investigations, routine pathologic assessments are subjected to large interobserver variability, making clinical decisions uncertain.[1] Furthermore, to enable unambiguous assessment of stage, for example, high-quality transurethral resection of bladder tumor samples that include muscle tissue is necessary. However, pathologic assessment alone is not sufficient to capture the underlying heterogeneity believed to exist among urothelial carcinomas such as T1 tumors. Accumulating molecular data support the existence of two broad pathogenetic subtypes of urothelial carcinoma that largely correspond to non—muscle-invasive and muscle-invasive tumors, respectively.[2] Non—muscle-invasive tumors typically exhibit frequent fibroblast growth factor receptor 3 (*FGFR3*) and PI3-kinase catacytic subunit α (*PIK3CA*) mutations, few chromosomal changes, and low mitotic or MKI67 (antigen Ki-67) activity. The more aggressive muscle-invasive tumors typically exhibit tumor protein p53 (*TP53*) mutations, high proliferative activity, and signs of genomic instability. Using gene expression profiling, we have recently shown that urothelial carcinoma may be divided into two major molecular subtypes, MS1 and MS2.[3] In a subsequent study, and using a larger set of tumors, further divisions were possible, resulting in a molecular taxonomy with four subtypes of urothelial carcinoma with

Supported by The Swedish Cancer Society, The Swedish Research Council, The Nilsson Cancer Foundation, and BioCARE.

http://dx.doi.org/10.1016/j.ajpath.2013.05.013

distinct molecular properties: urobasal A (UroA), urobasal B (UroB), squamous cancer cell−like (SSCL), and genomically unstable (GU) tumors.[4] The subtypes demonstrate distinct survival patterns in which UroA tumors are associated with a good prognosis, and UroB and SCCL tumors with the worst outcome. The suggested molecular classification shows only a moderate overlap with pathologic grade and stage. For example, at the molecular level, T1G3 tumors were classified as any of the four subtypes and muscle-invasive tumors as UroB, SCCL, or GU. Hence, our molecular taxonomy based on mRNA gene expression profiling refines the classification of urothelial carcinoma into subtypes with potential clinical effect. In the present investigation, we applied a large number of immunohistochemistry (IHC) markers to a cohort previously classified by available gene expression array profiling data and made a thorough molecular pathologic characterization of the suggested subtypes. Moreover, we demonstrated that a simple classifier that combines markers for basal cell status (KRT5, or cytokeratin 5) and proliferation (CCNB1, or cyclin B1), along with two histologic or morphologic variables, reproduced the three major molecular subtypes of urothelial carcinoma: UroA and UroB, GU, and SCCL.

Materials and Methods

Patient and Sample Selection

Tumor biopsy samples from 237 patients with urothelial carcinoma diagnosed at the Southern Sweden Health Care Region between 2001 and 2009 were included. From an original cohort of 308 cases previously analyzed by us using whole genome expression analysis,[4] we excluded 42 cases of the infiltrated subtype and 29 for which material for tissue microarray analysis (TMA) was not available. Patient and tumor data are given in Supplemental Table S1. The investigation was approved by the Regional Ethics Committee (first received date February 25, 2010; ref. No. 2010/5).

Tissue Microarrays and IHC

TMA blocks were constructed from 1.0 mm punches of formalin-fixed paraffin-embedded urothelial carcinoma specimens using a manual arrayer (Pathology Devices, Inc., Westminster, MD). Except in six cases, two cores per sample were included. From TMA blocks, tissue sections (3 to 4 μm thick) were mounted on glass slides (SuperFrost Plus; Gerhard Menzel GmbH, Braunschweig, Germany), dried at room temperature, and incubated for 2 hours at 60°C. Slides were pretreated using the PT Link Kit (pH 9) (Dako AS, Glostrup, Denmark). Antibody staining was performed using an Autostainer Plus (Dako). Standard incubation time was 30 minutes. Visualization of stained slides was performed using EnVision FLEX K8010 (Dako). Slides were counterstained with Mayer's hematoxylin for 2 minutes, and then were dehydrated.

Antibodies and IHC Evaluations

Antibodies used, product numbers, vendors, and dilutions for each primary antibody are given in Table 1. Cores were evaluated blinded as digitalized image files (ScanScope; Aperio, Vista, CA) by two independent investigators (G.S. and M.H.). For CCND1 (cyclin D1), CCNE1 (cyclin E1), CDH1 [E-cadherin (E-Cad)], epidermal growth factor receptor (EGFR), ERBB2 (Her-2), FGFR3, KRT5, KRT6 (cytokeratin 6), KRT14 (cytokeratin 14), KRT20 (cytokeratin 20), CDH3 [P-cadherin (P-Cad)], CDH2 [N-cadherin (N-Cad)], DSC2/3 (desmocollin 2/3), E2F3 (E2F transcription factor 3), RB1 (retinoblastoma 1), cyclin-dependent kinase inhibitor 2A, isoform 1 (CDKN2A), and uroplakin 3 (UPK3), the labeling intensity was assigned as no, low, moderate, or high expression (0 to 3, respectively). Tumor cell score (TCS) was defined as intensity multiplied by the fraction of positive tumor cells in 10% intervals. For CCNB1, MKI67, and tumor protein p63 (TP63), only the fraction of positive tumor cell nuclei was recorded. Because intensity cutoffs must be set individually for each marker, we have shown representative images in the Supplemental Appendix. For each case and each antibody, the mean TCS of core pairs from the same sample was calculated, and all IHC data are given in Supplemental Table S2. The number of cases with high difference between core pairs in intensity ($\Delta I \geq 2$) or tumor cell score ($\Delta TCS \geq 2$) was used as a measure of concordance and is given in Table 1. The number of core pairs evaluated for each marker ranged from 194 to 217. Downloadable IHC images in PDF format for all cases are available on request.

Histopathologic Evaluation

Tumor stage and grade were evaluated using the World Health Organization 1999 classification system. Three types of histologic annotations were made: invasive growth pattern, urothelial-like or not, and histologic variant. Examples of each type of histologic annotation are shown in Supplemental Figure S1. Growth patterns in invasive tumors were recorded as nodular, trabecular, or infiltrative using the definitions provided by Jimenez et al[5] (Supplemental Figure S1, A−C) The term *urothelial-like* was used to denote tumors with stroma separated from the tumor cells by a smooth undisrupted basal interface, an overall organized tumor parenchyma, and nuclei of relatively similar form and size (Supplemental Figure S1D). The annotation urothelial-like was given to tumors that fulfilled all of these criteria. α-Smooth muscle actin (ACTA2) staining was used to evaluate the integrity of the tumor-stroma interface. The presence of histologic variants was recorded as signs of squamous and glandular differentiation (Supplemental Figure S1, F and G).[6−8] Signs of squamous differentiation considered included polygonal cell shape; distinct cell borders; high cytoplasm/nucleus ratio; presence of desmosomes (aided by DSC2/3 staining), keratinization, visible as

Table 1 Antibody Information, Concordance between Duplicate Cores, and Correlation With mRNA Levels

Marker	Catalog No.	Vendor	Dilution	ΔI ≥2*	ΔTCS ≥2†	TCS-GEX r‡	P‡
CCNB1	1495-1	Epitomics	1:100	NA	7 (3.3)	0.6	3.1×10^{-25}
CCND1	M3635	Dako	1:100	15 (7.0)	1 (0.5)	0.56	1.4×10^{-21}
CCNE1	NCL-CYCLIN E	Leica	1:60	26 (12.4)	2 (1.0)	0.63	9.5×10^{-28}
CDH1	M3612	Dako	1:200	16 (7.5)	11 (5.1)	0.28	6.7×10^{-6}
CDH2	33-3900	Invitrogen	1:100	12 (5.5)	3 (1.4)	0.54	1.2×10^{-19}
CDH3	#610228	BD Biosciences	1:200	21 (10.0)	7 (3.3)	0.46	5.3×10^{-14}
CDKN2A	#550834	BD Biosciences	1:50	9 (4.2)	7 (3.3)	0.56	6.3×10^{-22}
DSC2/3	C228807	LifeSpan	1:35	2 (1.0)	2 (1.0)	0.4	6.9×10^{-11}
E2F3	MS-1063	Lab Vision	1:80	15 (7.4)	0 (0)	0.45	9.2×10^{-14}
EGFR	790-2991	Ventana	RTU	19 (8.8)	10 (4.6)	0.47	4.5×10^{-15}
ERBB2	790-2991	Ventana	RTU	7 (3.3)	6 (2.8)	0.49	5.2×10^{-16}
FGFR3	#4574	Cell Signaling	1:40	10 (4.8)	10 (4.8)	0.65	1.6×10^{-30}
KRT14	MS-115	Lab Vision	1:200	14 (6.6)	2 (0.9)	0.64	1.1×10^{-29}
KRT20	M7019	Dako	1:500	29 (14.4)	19 (9.5)	0.61	8.8×10^{-26}
KRT5	RM-2106	Lab Vision	1:200	37 (17.6)	5 (2.4)	0.72	1.6×10^{-39}
KRT6	MS-766	Lab Vision	1:200	10 (4.7)	9 (4.2)	0.42	3.8×10^{-12}
MKI67	RM-9106	Lab Vision	1:500	NA	14 (6.8)	0.62	1.0×10^{-26}
RB1	#9309	Cell Signaling	1:100	8 (3.8)	4 (1.9)	0.44	4.0×10^{-13}
TP63	IMG-80212	Imgenex	1:100	NA	29 (13.6)	0.73	1.9×10^{-41}
UPK3	AIB-30180	Nordic Biosite	1:20	36 (17.2)	4 (1.9)	0.19	0.0013

*Number and percentage of tumors showing a large difference in intensity between cores from the same sample.
†Number and percentage of tumors showing a large difference in TCS between cores from the same sample.
‡Correlation between TCS and relative mRNA levels indicated by Pearson r and corresponding P values.
NA, not available.

intracellular or extracellular material with bright homogeneous staining (aided by KRT5 and KRT14 staining); presence of apoptotic ink-cells; and brightly stained nuclei (H&E) with clearly visible nucleoli. Signs of glandular differentiation considered included tubular structures and columnar cells, glandular spaces within the tumor mass, mucin-containing cells, and decreased thickness of cell layers. The group of SCCL tumors was originally defined by their gene expression profile, which shows high expression of genes involved in keratinization characteristic of normal squamous tissue. Most SCCL tumors also showed histologic signs of squamous differentiation in whole tissue sections.[4]

Tumor Classification

For potential variables to include in a classifier we considered IHC markers with strong distinctive staining (CCNB1, CCND1, CDH1 (E-Cad), CDH3 (P-Cad), CDKN2A, DSC2/3, EGFR, ERBB2, FGFR3, KRT5, KRT14, MKI67, and TP63), along with sex, tumor grade, urothelial-like histologic findings, invasive growth pattern, and squamous or glandular differentiation. We also considered marker stratification in relation to tumor stroma. The classifier was constructed in a treewise fashion starting with the division urobasal versus GU/SCCL, and then subdivisions for UroA versus UroB and GU versus SCCL. For reliable use across laboratories, we decided to dichotomize all numerical features to 0 or 1 using a threshold. Optimal cutoffs were determined via receiver operating characteristic analyses using the R packages *ROCR*[9] and *rocc*[10]. For categorical variables, we evaluated all possible dichotomization options, and values were set at 0 or 1. Dichotomized variables were then ranked by association to true class measured using the Fisher exact test, and the top ranked feature was selected. Additional features were added if the P value from multivariate logistic regression (true class dependent on features) added significant information to the already selected features ($P = 0.001$). Only three IHC markers were allowed, and five features overall, restricting the feature selection method to few markers that carry independent information. The classification score was defined as the sum of feature values for a division and ranged from 0 to the number of features included. Receiver operating characteristic analyses were used to determine the best classification score cutoff in each division. A new sample is classified along the classification tree as being above or below the classification score cutoff in each division (for full classifier structure, see Supplemental Figure S2). To estimate the accuracy of our classification system, we used leave-one-out cross-validation comparing classifications with the true sample classes as determined via previous genomewide gene expression analyses.[4] We then assessed the effect of additional makers on classification accuracy. To include more markers, we relaxed the P value from multivariate logistic regression in feature selection from $P = 0.001$ to $P = 0.01$ and $P = 0.05$. In the first division, CCND1 (classifier B, $P = 0.01$) and MKI67 (classifier C, $P = 0.05$) were included. For the division of SCCL versus GU, no marker provided additional information in the extended models. Classification accuracy in leave-one-out cross-validation was 0.884, 0.879, and 0.879 for the original classifier, classifier B,

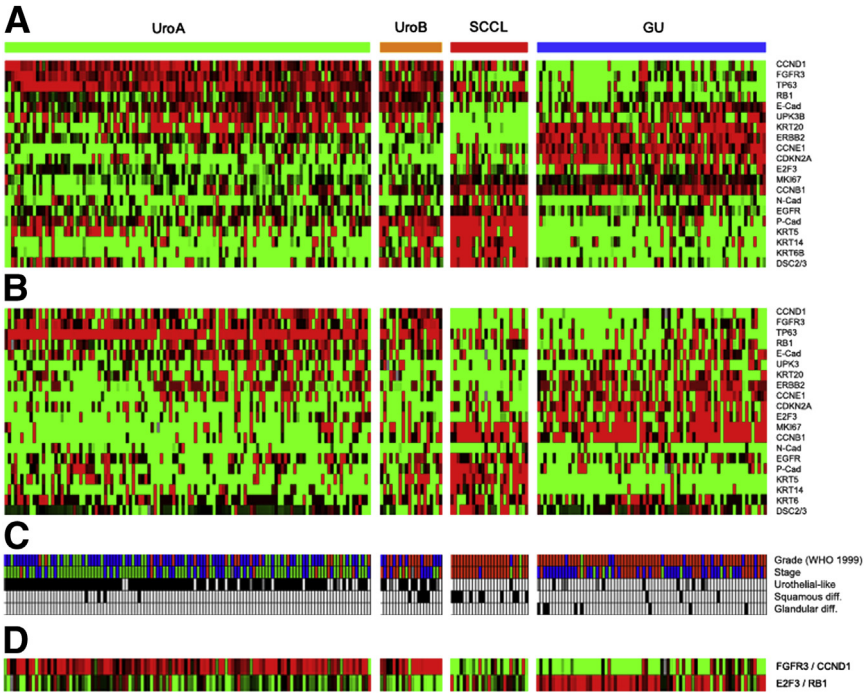

Figure 1 **A:** Heat map of mRNA expression levels for 19 of 20 selected genes. Heat map is based on data published by Sjödahl et al[4] **B:** Heat map of relative IHC TCS or fractions of positive cells, both standardized across cases. **C:** Distribution of pathologic stage, grade, urothelial-like growth pattern, and signs of squamous and glandular differentiation in molecular subytpes. For stage and grade, respectively, green bars indicate Ta or G1 tumors, blue bars indicate T1 or G2 tumors, and red bars indicate ≥T2 or G3 tumors. Black bars indicate urothelial-like growth pattern and signs of squamous or glandular differentiation. Gray bars represent missing data. **D:** Expression of FGFR3/CCND1 and E2F3/RB1 genomic circuits across samples. Casewise scores for the respective circuits are calculated as described in *Material and Methods*.

and classifier C, respectively. Hence, adding more markers resulted in similar classifier performance.

Statistical Analysis

The Fisher exact test was used to test differences in proportions of categorical data. Differences in intensity and TCS were evaluated using U tests. The urothelial carcinoma–specific genomic circuits were adapted from Lindgren et al.[11] Genomic circuit scores were calculated as FGFR3/CCND1 circuit = $TCS_{FGFR3} + TCS_{CCND1} - TCS_{P16}$, and E2F3/RB1 circuit = $TCS_{E2F3} + TCS_{P16} - TCS_{RB1}$. For clinical associations, Kaplan-Meier analyses and Cox regression with the log-rank test for significance were used.

Results

IHC Markers

We constructed tissue microarrays from 237 urothelial carcinomas previously classified into the four molecular subtypes UroA ($n = 118$), UroB ($n = 20$), SCCL ($n = 25$), and GU ($n = 74$) using gene expression profiling.[4] Twenty genes were selected as possible class-defining IHC markers (Figure 1A). The intensity scoring showed overall good concordance between core pairs from the same biopsy sample (Table 1). However, because the TCS showed better concordance, this measure was primarily used in the subsequent analyses. Correlations between mRNA expression and TCS ranged between 0.42 and 0.73, with CDH1 (E-Cad) and UPK3 as outliers ($r < 0.30$) (Table 1). Overall, the IHC results were in good concordance with those obtained via mRNA gene expression analyses (Figure 1, A and B).

Molecular Pathologic Characterization

UroA Tumors

Most UroA tumors were non–muscle-invasive (92%), of low grade (G1 or G2) (86%), and with urothelial-like histologic features (86%) (Table 2 and Figure 1C). FGFR3 showed homogeneous staining in all tumor cells in 92% of UroA samples. The most luminal cell layer, when present in the TMA cores, was consistently negative for TP63, whereas intermediate and basal cell layers were positive (Figure 2A). CCND1 showed nuclear staining and ranged from being expressed in the suprabasal cell layer only to including all tumor cells, resulting in strong but variable CCND1 expression. A total of 96% of tumors were positive for CCND1 expression. In general, the fractions of $CCND1^+$ cells were larger than for $CCNB1^+$ or $MKI67^+$ cells.

KRT5 expression was observed in 106 tumors (91%) and was restricted to the basal cell layer in 49% of tumors (Figure 2A). An almost identical pattern with positive cells confined to the basal cell layer was noted for CDH3 (P-Cad). In contrast, CDH1 (E-Cad) expression was detected in all cell layers and in 98% of UroA tumors. CDH2 (N-Cad) expression was absent in 75% of UroA tumors and was expressed at very low levels when positive. Thus, cadherin-mediated epithelial cell-cell adhesion is not altered in UroA tumors compared with normal urothelium. CCNB1 expression was limited to the suprabasal cell layer in most UroA tumors (Figure 2A). $CCNB1^+$ cells were typically elongated and in contact with the tumor-stroma interface. MKI67

Table 2 Tumor Pathologic Characteristics and Growth Patterns

Variable	UroA* (n = 118)	UroB* (n = 20)	SCCL* (n = 25)	GU* (n = 74)
Stage†				
Ta	78 (66)	4 (20)	2 (8)	8 (11)
T1	31 (26)	6 (30)	1 (4)	40 (54)
≥T2	8 (7)	9 (45)	22 (88)	26 (35)
Tx	1 (1)	1 (5)	0	0
Grade†				
G1	33 (28)	0	1 (4)	1 (1)
G2	68 (58)	9 (45)	1 (4)	10 (14)
G3	17 (14)	11 (55)	23 (92)	63 (85)
Growth pattern‡				
Urothelial-like	99/115 (86)	11/18 (61)	1/25 (4)	6/68 (9)
Not urothelial-like	16/115 (14)	7/18 (39)	24/25 (96)	62/68 (91)
Infiltrative	1/116 (1)	4/20 (20)	10/25 (40)	18/74 (24)
Nodular	2/116 (2)	0	1/25 (4)	5/74 (7)
Trabecular	0	2/20 (10)	9/25 (36)	11/74 (15)
Histologic variant‡				
Squamous	4/116 (3)	5/20 (25)	11/25 (44)	3/74 (4)
Glandular	0	0	0	8/74 (11)

Values are given as No. (%).
*Molecular subclass according to whole genome gene expression.[4]
†Determined via pathologic evaluation of paraffin-embedded tissue from whole tissue sections.
‡Determined using TMA sections.

showed a labeling pattern similar to CCNB1 but with less pronounced stratification, confirming that most of the proliferation in UroA tumors occurs in the basal and suprabasal cell layers.

KRT20 and UPK3 expression is restricted to the most luminal cells in normal urothelium. However, KRT20 showed aberrant expression, localized to the tumor interior in 56% of tumors and to UPK3 in 35% of tumors. Only two tumors (2%) showed KRT20 expression reminiscent of normal urothelium. UPK3 expression in the apical membrane of the most luminal cells was noted in 44% of tumors.

UroB Tumors

About half of the UroB tumors were muscle-invasive. Eleven tumors demonstrated urothelial-like histologic characteristics, and five tumors showed histologic signs of squamous differentiation (Table 2). Similar to UroA tumors, FGFR3 and CCND1 were expressed in 80% and 90% of tumors, respectively, and TP63 was expressed in most (>70%) cells in 80% of UroB tumors. KRT5 expression was restricted to the basal cell layer in only two tumors (10%), compared with 49% in UroA tumors ($P < 0.002$). KRT14 was expressed in 30% of UroB tumors, compared with 9% of UroA tumors ($P < 0.01$) (Figure 2B) and was confined to the basal cell layer when expressed. There was no major difference in cadherin expression between UroA and UroB tumors (Figure 3). Of 13 tumors that could be evaluated for CCNB1, basal or suprabasal expression was observed in 9 and in all cell layers in 4. MKI67 exhibited a similar expression pattern. However, compared with UroA tumors, UroB tumors demonstrated a significantly larger fraction of $CCNB1^+$ and $MKI67^+$ cells, indicating a higher proliferation index (Figure 4). KRT20 showed aberrant expression in 47% of UroB tumors and was completely negative in the remaining tumors. UPK3 expression was absent in 80% of tumors.

SCCL Tumors

Most SCCL tumors were muscle-invasive, of high grade, and showed various invasive growth patterns (Table 2). Morphologic signs of squamous differentiation were noted in 11 tumors (44%). Strong membrane DSC2/3 staining, a marker for squamous differentiation, was noted in 67% of SCCL tumors, compared with 7% of UroA and 30% of UroB tumors (Figure 5A). FGFR3 positivity was observed in 6 of 25 tumors, of which 3 showed expression close to the detection level. Moreover, TP63 expression was observed in significantly fewer SCCL tumors compared with UroA and UroB tumors ($P < 3 \times 10^{-6}$). Similarly, CCND1 was negative or showed low expression in 84% of SCCL tumors (Figure 5A). In contrast, EGFR expression was stronger than in UroA tumors ($P = 8 \times 10^{-4}$), noted in 96% of SCCL tumors, and was not restricted to the basal cell layers as in UroA tumors (Figures 3 and 5A).

SCCL tumors showed strong KRT5 expression throughout the tumor parenchyma in 92% of cases. Of importance, stroma-adjacent cells did not show stronger KRT5 expression when compared with cells not in contact with stroma (Figure 5A). KRT14 and KRT6, not normally expressed in the urothelium or in the other subtypes of urothelial carcinoma, showed expression in 76% and 24% of tumors, respectively. In most positive tumors, KRT14 expression was moderate to strong and not limited to stroma-adjacent cells. KRT20 positivity was noted in only 3

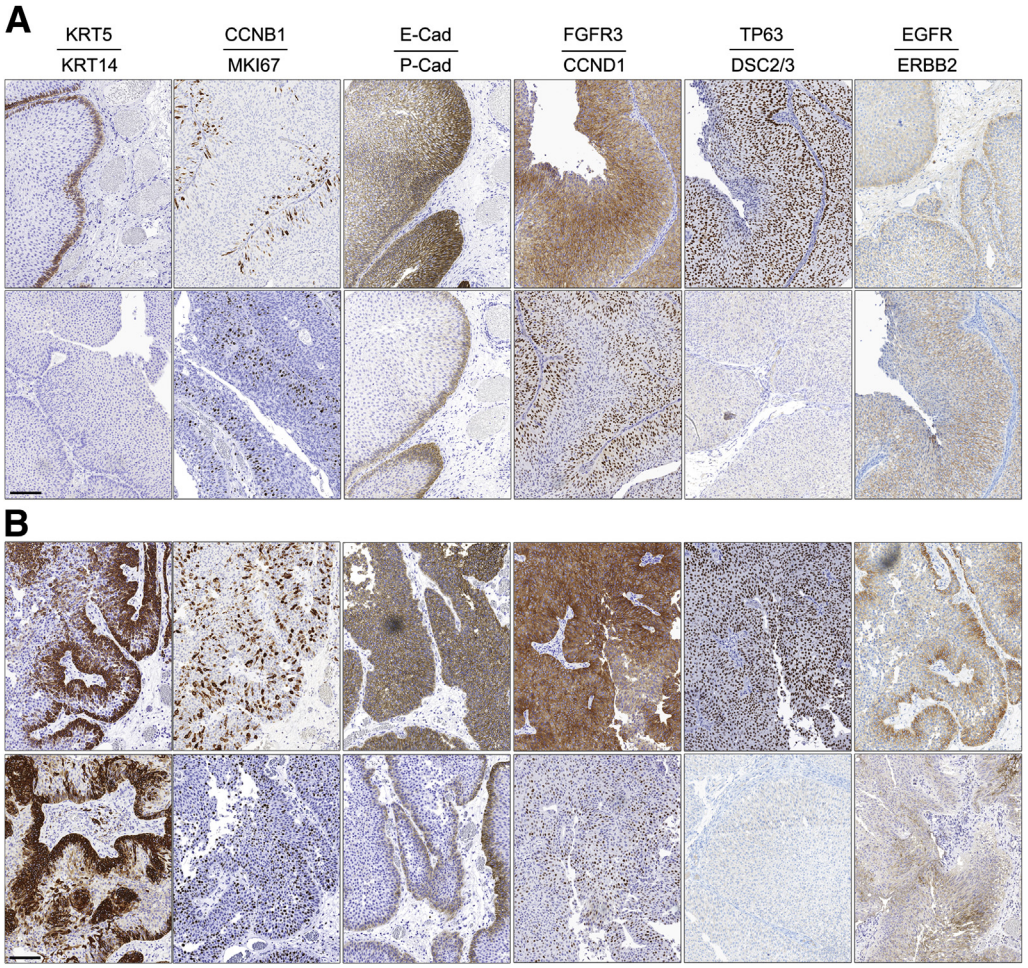

Figure 2 Examples of IHC results for UroA tumors (**A**) and UroB tumors (**B**). Scale bars: 100 μm.

tumors, and UPK3 in 10 of 25 tumors, all with aberrant expression patterns. CCNB1 and MKI67 expression was observed throughout the tumor parenchyma, indicating that proliferation was not restricted to stroma-adjacent cells (Figure 5A). CCNB1 and MKI67 expression was significantly higher in SCCL tumors than in UroB tumors, indicating high proliferative activity (Figure 4). E-Cad expression was completely absent in 5 of 24 SCCL tumors and was significantly lower than in UroA and UroB tumors ($P = 3 \times 10^{-7}$). In contrast, CDH3 (P-Cad) showed significantly stronger staining ($P = 10^{-6}$) in SCCL compared with UroA and UroB tumors and all through the tumor parenchyma (Figurse 3 and 5A). Only 2 of 25 SCCL tumors (8%) showed CDH3 (P-Cad) expression restricted to cells at the tumor-stroma interface, compared with 50% to 60% of UroA or UroB tumors.

GU Tumors

GU tumors were typically high grade (G3) and T1 or muscle-invasive (Table 2). Half showed an invasive growth pattern, and only six (9%) exhibited urothelial-like histologic features. Signs of glandular differentiation were observed in the GU subtype only (Table 2). GU tumors were negative or showed low intensity for FGFR3 (Figure 3 and Figure 5B). Similarly, most tumors (63%) were negative for CCND1 expression (Figure 3), and when detected, expression was lower than in UroA and UroB tumors ($P = 0.007$) and was observed throughout the tumor parenchyma. TP63 expression was absent in 22% of GU tumors, and when positive, only 35% showed labeling of most of the cells (>70%), compared with 95% in UroA tumors ($P = 1 \times 10^{-19}$). Hence, low FGFR3, CCND1, and TP63 expression is a shared feature of GU tumors. Similarly, EGFR expression was significantly lower than in SCCL tumors ($P = 0.001$) (Figure 3). In contrast, GU tumors exhibited higher ERBB2 expression than did SCCL ($P = 3.1 \times 10^{-7}$), UroA ($P = 2.4 \times 10^{-5}$), and UroB ($P = 0.0017$) tumors (Figure 3). The vast majority of GU tumors were $KRT5^{-}$ and $KRT14^{-}$ (Figure 3), and when detected, expression was noted in isolated or small clusters of cells. KRT6 was not expressed in any tumors. Aberrant KRT20 and UPK3 were, however, frequently observed, in 72% and 51% of tumors, respectively. Similar to SCCL tumors, GU tumors showed high proliferative activity (Figure 4), with no stratification of $CCNB1^{+}$ and $MKI67^{+}$ cells (Figure 5B). In contract to SCCL tumors, GU tumors demonstrated low

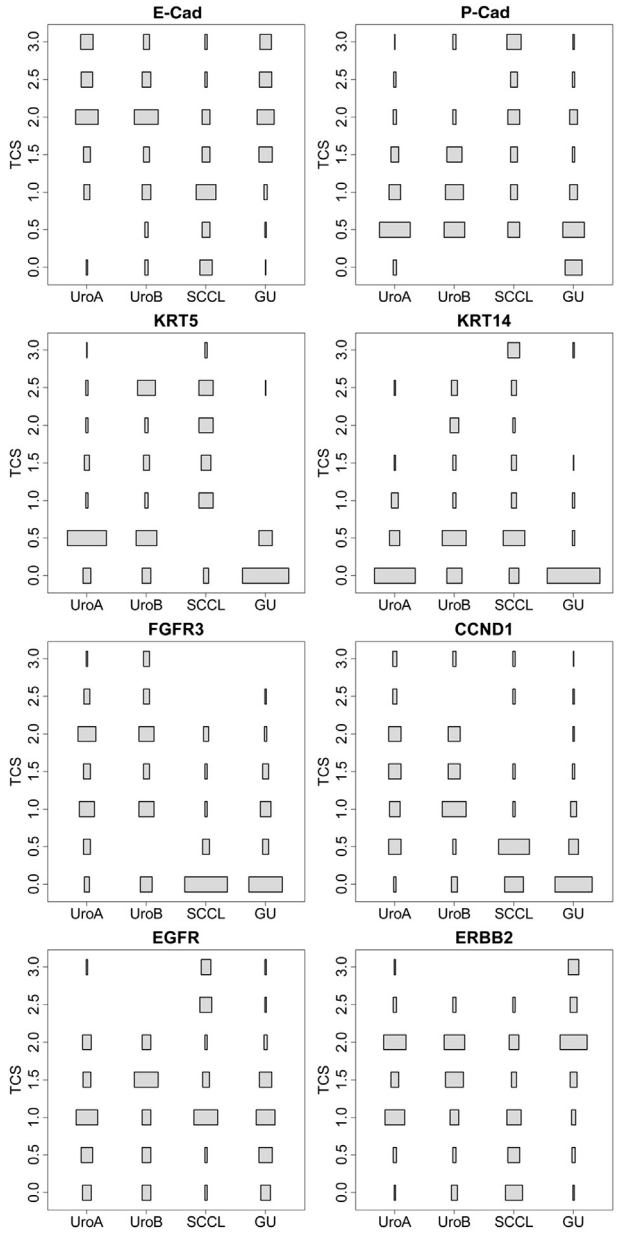

Figure 3 Proportional expression plots. Distribution of expression levels for individual markers within each tumor subtype. Each box is proportional to the fraction of tumors showing a TCS at the indicated level. Maximum TCS = 3, minimum TCS = 0, and sum of box areas for each tumor subtype = 1.

CDH3 (P-Cad) but high CDH1 (E-Cad) expression (Figure 3). IHC results for all molecular subtypes are summarized in Figure 6.

Urothelial Carcinoma–Specific Genomic Circuits Are Also Detected at the Protein Level

By combining information on genomic alterations and mRNA gene expression, we recently defined two genomic circuits operative in urothelial carcinoma.[7] One circuit, *FGFR3/CCND1*, was defined in part by high *FGFR3* and *CCND1* but low *CDKN2A* (p16) expression. The latter was frequently associated with homozygous deletions of the *CDKN2A* gene.[7] The second circuit, *E2F3/RB1*, was defined in part by *E2F3* genomic amplifications and high expression, *RB1* deletions and low expression, and high *CDKN2A* (p16) expression. Using available IHC data, we calculated a score for each of the two circuits assigned to each case (see *Material and Methods*). The two circuits were also detected at the protein level, and the FGFR3/CCDN1 circuit was operative in UroA and UroB tumors, whereas the E2F3/RB1 circuit was operative in GU tumors, SCCL being unassigned (Figure 1D). These results stress the close biological relationship between UroA and UroB tumors.

Molecular Pathologic Classification

We then constructed a tumor classifier using the most informative IHC, histologic, and morphologic variables. Using only four variables (urothelial-like histologic features, pathologic grade, CCNB1 >17% positive cells, and KRT5 tumor cell score >0.57), the original whole genomewide gene expression classification into UroA, UroB, SCCL, and GU tumors was reproduced with an overall accuracy of 0.88 and with excellent sensitivity and positive prediction values (Supplemental Figure S2 and Table 3). Attempts to subdivide the urobasal subtype into UroA and UroB were made; however, no acceptable division was obtained using the available markers. Of the 18 UroB tumors included in the analysis, 11 were classified as urobasal, 5 as SCCL, and 2 as GU. In agreement with good classification accuracy, the urobasal group was identified as associated with a good prognosis, the GU group with an intermediate outcome, and the SCCL with an unfavorable prognosis, using disease-specific survival as an endpoint and Kaplan-Meier analysis ($P = 4 \times 10^{-7}$) (Figure 7), in full accordance with previous results obtained with whole genome gene expression analysis.[4]

Discussion

In the present investigation we show that the four molecular subtypes of urothelial carcinoma, formerly suggested by whole genome gene expression analysis, demonstrate

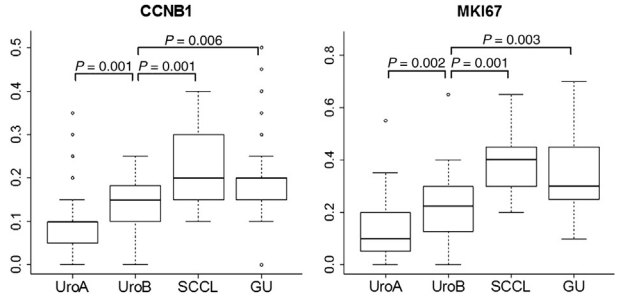

Figure 4 Boxplots showing the fractions of cells positive for proliferation markers CCNB1 and MKI67 in the tumor subtypes.

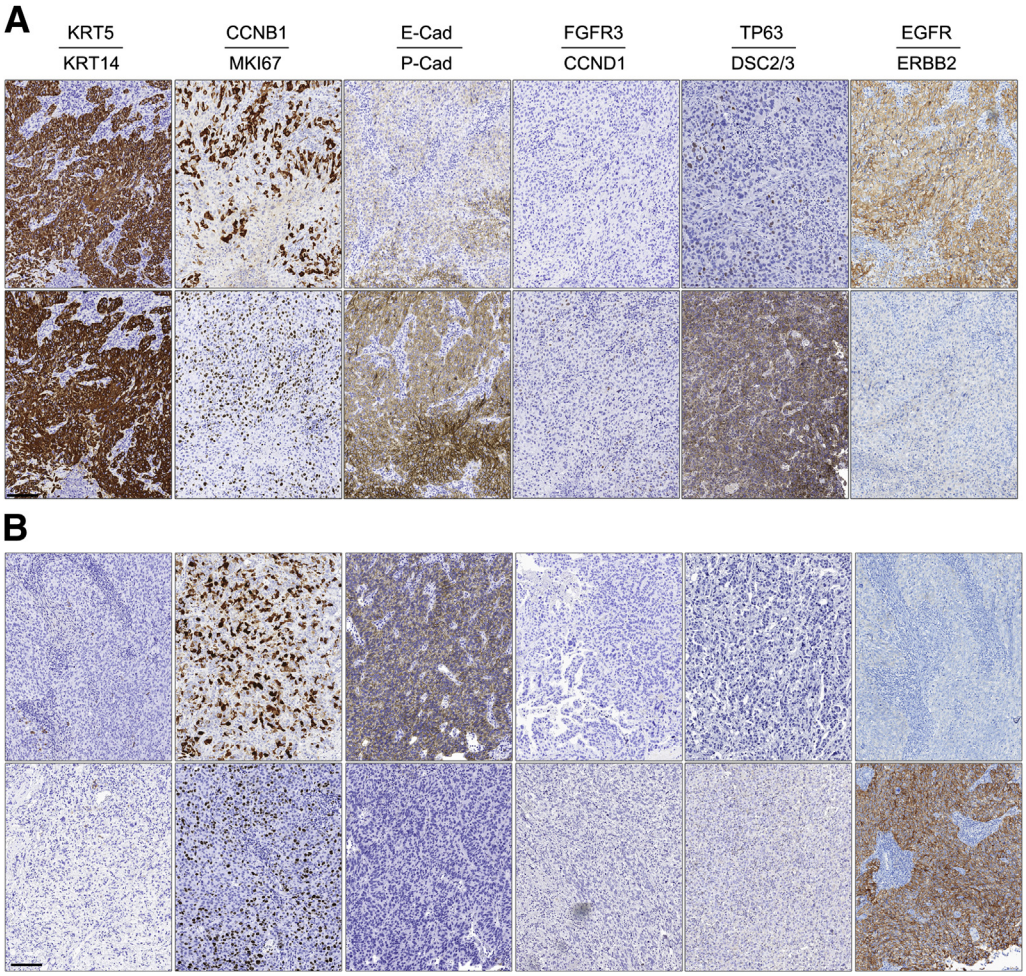

Figure 5 Examples of IHC results for SCCL (**A**) and GU (**B**) tumors. Scale bar = 100 μm.

distinct features at the molecular pathologic level. The infiltrated group of tumors was omitted from the present analyses because this group shows a high content of infiltrating immunologic cells[4] and thus does not represent a phenotype intrinsic to the tumor cells. The relationship between tumor molecular subtype and infiltrating immunologic cells is discussed elsewhere (Sjödahl et al, unpublished results). Marker genes were selected on the basis of the mRNA expression pattern in the context of the molecular subtypes UroA, UroB, SCCL, and GU. To facilitate an integrated molecular pathologic analysis, the marker genes were selected to include different aspects of cellular function such as cell cycle activity (CCNB1 and MKI67), cell-cell interactions (E-Cad, N-Cad, P-Cad, and DSC2/3), cellular architecture (KRT5, KRT6, and KRT14), and tyrosine kinase receptors (FGFR3, ERBB2, and EGFR). We next classified individual tumors with high accuracy into the three major molecular subtypes using a combination of only two IHC markers, urothelial-like histologic findings and pathologic grade. This makes the classification system easy to implement in the standard pathologic evaluation of urothelial carcinoma. Survival analyses showed that this classification system successfully reproduced our previous results obtained using mRNA gene expression arrays.

UroA tumors showed a labeling pattern reminiscent of normal urothelium for several markers. KRT5, CDH3 (P-Cad), and EGFR showed distinct labeling of cells adjacent to the basal membrane, thus differentiating the basal cell layers from the remaining tumor cells. UroA also showed extended and smooth stromal interfaces, indicating a maintained tumor-stroma hierarchical organization; eg, palisading of basal cells was frequently seen. Expression of TP63, involved in epithelial stratification, in stroma-adjacent cells and throughout the tumor parenchyma except for the most luminal cells is compatible with what is observed in normal urothelium. Cell proliferation, as determined by CCNB1 and MKI67, was primarily detected adjacent to the stroma, suggesting possible dependence of the basal membrane for proliferation. Indeed, CCNB1-labeled cells were observed protruding from and frequently in contact with the tumor-stroma interface. CCND1, which also is a driver of the cell cycle, showed suprabasal labeling that extended into the tumor parenchyma, sometimes including all tumor cells, thus producing an overall stronger CCND1 staining pattern than observed

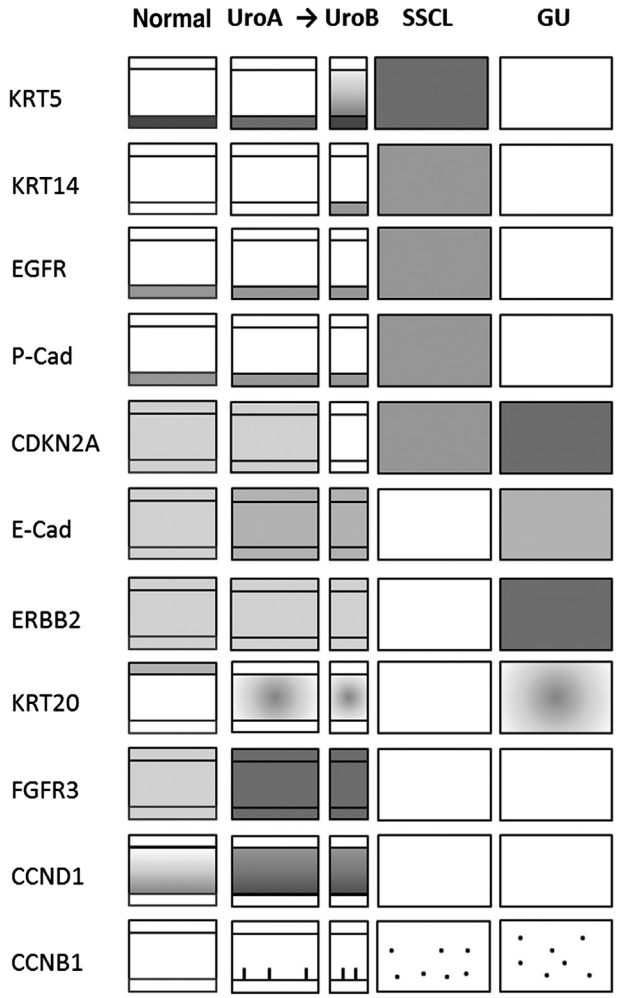

Figure 6 Schema of IHC results for selected markers. Normal indicates expression pattern in normal urothelium. Urobasal tumors are divided into UroA and UroB and are schematically drawn with a basal cell layer, intermediate cells, and luminal cells. Dark shading indicates strong expression. For CCNB1, single cells protruding from the tumor-stroma interface are indicated by lines, and positive cells within the tumor parenchyma as dots. Centered shading for KRT20 indicates aberrant expression frequently seen in the center of the tumor parenchyma.

in normal urothelium. Emerging findings indicate that UroA tumors are driven by increased proliferative activity of cells in close proximity to the stroma/basal membrane boundary, thus resembling the pattern of proliferation and cell turnover observed in normal urothelium.

In contrast, the differentiation markers KRT20 and UPK3 frequently showed aberrant expression. In particular, KRT20 expression was often observed in the interior of the tumor parenchyma, supporting the observation by He et al[12] that KRT20 may be aberrantly expressed within the tumor parenchyma as a function of distance from the stromal compartment. Luminal cells, when present in cores, frequently shared morphologic features with umbrella cells, even when KRT20$^-$ or UPK3$^-$. These findings suggest a compromised differentiation process in UroA with only parts of the original differentiation program in operation.

Table 3 Results of IHC/Histopathology Classification

Variable	Uro (IHC*)	SCCL (IHC)	GU (IHC)	Sensitivity†
UroA/UroB (GEX‡)	115	6	11	0.87
SCCL (GEX)	2	22	1	0.88
GU (GEX)	5	1	62	0.91
PPV§	0.94	0.76	0.84	

*Classification according to IHC/histopathology classifier using leave-one-out cross-validation.
†Sensitivity of IHC/histopathology classifier.
‡Classification according to whole genome gene expression.[4]
§PPV for IHC/histopathology classifier.
PPV, positive predictive value.

However, in large tumors with many cell layers, an aberrant differentiation program may be activated within the tumor parenchyma.

SCCL tumors showed staining patterns in strong contrast to those of UroA tumors. KRT5, CDH3 (P-Cad), and EGFR expression, limited to the basal cell layer in UroA tumors, in SCCL tumors was detected throughout the tumor parenchyma and with higher intensity. Consequently, SCCL cells seem to have acquired properties similar to those of basal cells in normal urothelium and could thus be denoted as basal-like. Inasmuch as the SCCL class of tumors was distinguished by being KRT14$^+$, KRT5$^+$, and KRT20$^-$, this group conforms to the basal category of tumors described by Volkmer et al[13] and also by Chan et al[14] However, in contrast to basal cells of UroA tumors, the basal-like character of SCCL cells is independent of direct contact with stroma. Furthermore, the SCCL subtype of urothelial cancer shows an IHC marker profile similar to the basal-like phenotype in breast carcinomas.[15] This again stresses the similarity of SCCL tumors to undifferentiated basal-like cells.[16] Proliferation, as detected by CCNB1 and MKI67, was substantially stronger than in UroA tumors, was observed throughout the tumor parenchyma, and was not topologically constrained as in UroA tumors.

Tumor cell proliferation in GU tumors was noted throughout the tumor parenchyma. However, in contrast to SCCL tumors, GU tumors did not express KRT5, KRT14, or KRT6 and showed high CDH1 (E-Cad) but low CDH3 (P-Cad) expression. Our results are in agreement with previous analyses that related cadherin expression pattern to tumor stage and grade.[17] GU tumors also differed distinctly from UroA tumors by showing absence of or strongly deranged urothelial-like stratification. A characteristic feature of many GU tumors was lack of or low expression of most markers in the panel, with the exception of ERRB2, CCNB1, MKI67, and CDH1 (E-Cad). Hence, GU tumors correspond to undifferentiated high-grade cells with a strong proliferative potential. A critical difference between UroA tumors and SCCL and GU tumors seems to be the apparent independence of cell proliferation from the stroma/basal membrane in the latter two. We have previously shown that the change between UroA to SCCL and GU is accompanied

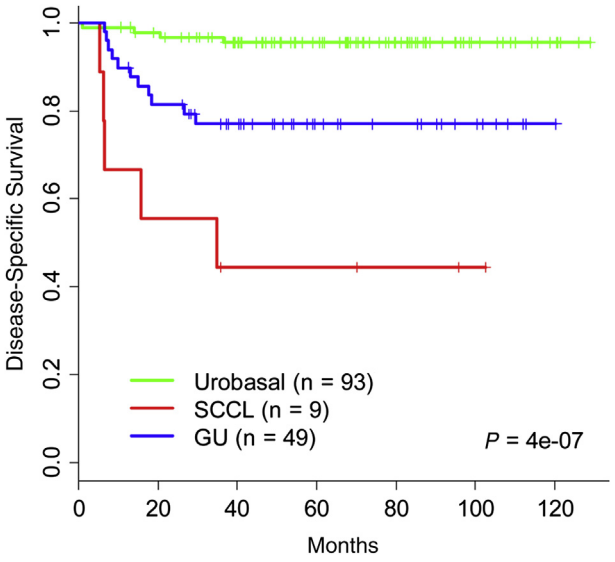

Figure 7 Kaplan-Meier plot of disease-specific survival. Tumors are stratified by molecular subtype as determined by the IHC/histology classifier. Classification was obtained through leave-one-out cross-validation.

by a transition from high expression of early cell cycle genes, in particular *CCND1*, to high expression of late cell cycle genes, eg, *CCNE1*.[4] Hence, independence of proliferation from the stroma/basal membrane may be a decisive shift in the progression of urothelial carcinoma.

UroB and UroA tumors share high expression of FGFR3, CCND1, and TP63 and a high *FGFR3* mutation frequency.[4] However, UroB tumors differ from UroA tumors in that they exhibit higher fractions of KRT5-expressing cells not necessarily restricted to the basal and suprabasal cell layers, a higher fraction KRT14$^+$ tumors, higher numbers of CCNB1$^+$ and MKI67$^+$ cells, and lower CDKN2A (p16) expression. Most important, half of the UroB tumors are muscle-invasive, which suggests that UroB tumors are a molecularly evolved version of UroA tumors. UroB tumors are most likely represented among the *FGFR3* mutated and *CDKN2A* homozygous deleted tumors with a bad prognosis described by Rebouissou et al[18] and the muscle-invasive tumors that have retained *TP63* expression described by Urist et al.[19]

We have recently identified two genomic circuits operative in urothelial carcinoma, the *FGFR3*/*CCND1* and *E2F3*/*RB1* circuits.[11] When translated into IHC markers, the FGFR3/CCND1 circuit produces high scores and the E2F3/RB1 circuit low scores in both UroA and UroB tumors, whereas the opposite is noted in GU tumors. These findings emphasize the distinct natures of UroA, UroB, and GU tumors and the close relationship between UroA and UroB tumors. Furthermore, the four subtypes show distinct expression of key receptor tyrosine kinases. UroA and UroB tumors show strong FGFR3 and moderate to low ERBB2 and EGFR expression. In contrast, SCCL tumors show almost absent FGFR3 and ERBB2 but strong EGFR expression, and GU tumors show almost absent FGFR3 and EGFR but strong ERBB2 expression. Together this identifies UroA and UroB, GU, and SSCL as three basic molecular pathologic subtypes of urothelial carcinoma.

In breast cancer, gene expression and IHC-based classification systems have been developed in parallel and have subsequently been successfully reconciled. The major intrinsic molecular subtypes of breast cancer were first identified by gene expression profiling[20] and later were translated into three main IHC-based subtypes using estrogen receptor, progesterone receptor, and HER2 antibodies. Additional IHC markers have been used to identify the molecular subtypes in greater detail: MKI67 to differentiate luminal A from luminal B and KRT5/6 and EGFR to identify the basal-like subtype among the estrogen receptor, progesterone receptor, and HER2 triple-negative tumors, reviewed by Blows et al.[21] To facilitate the translation of our suggested urothelial carcinoma molecular taxonomy into clinical practice, we used results for all 20 IHC markers, pathologic data (grade and stage), and information about growth pattern to establish a simple classification system. Selection of classifier variables was unsupervised, and care was taken to limit the number of markers. The final classifier arrived at included information on CCNB1 and KRT5 staining, pathologic grade, and urothelial-like growth pattern. Using these four markers, the three major molecular subtypes of urothelial cancer could be predicted with high fidelity. Furthermore, the IHC and histopathologic subtypes correspond to distinct groups with respect to prognosis. The small UroB group could not be identified as a separate group by using the selected set of markers. The difficulty in identification of the UroB subtype using the IHC or histologic classifier most likely results because the UroB group shares features with both the GU and SCCL subtypes, eg, invasiveness and high proliferation rate, and with UroA, eg, high FGFR3 expression and stratified KRT5 expression. Consequently, no single variable can easily be attributed to the class of UroB tumors. As a result, about half of UroB tumors were classified as low risk urobasal and half as high-risk GU or SCCL tumors. It must be stressed, however, that TMA was used in the present investigation and that better differentiation may have been attained using whole tissue sections. Irrespective, we noted that assessment of pathologic stage was not necessary to obtain excellent classification results. We argue that our suggested mRNA-based molecular taxonomy and the present IHC- and histopathology-based classification systems are promising tools for understanding urothelial cancer biology and for future bladder cancer management. We do, however, stress the importance of classifier validation in truly independent data with long-term follow-up and analysis via both IHC and histopathology and by genomewide gene expression.

Acknowledgment

We thank Tetsutaro Hayashi for suggesting the DSC2/3 antibody.

Supplemental Data

Supplemental material for this article can be found at *http://dx.doi.org/10.1016/j.ajpath.2013.05.013*

References

1. May M, Brookman-Amissah S, Roigas J, Hartmann A, Störkel S, Kristiansen G, Gilfrich C, Borchardt R, Hoschke B, Kaufmann O, Gunia S: Prognostic accuracy of individual uropathologists in noninvasive urinary bladder carcinoma: a multicentre study comparing the 1973 and 2004 World Health Organisation classifications. Eur Urol 2010, 57:850−858
2. Wu XR: Urothelial tumorigenesis: a tale of divergent pathways. Nat Rev Cancer 2005, 5:713−725
3. Lindgren D, Frigyesi A, Gudjonsson S, Sjödahl G, Hallden C, Chebil G, Veerla S, Ryden T, Månsson W, Liedberg F, Höglund M: Combined gene expression and genomic profiling define two intrinsic molecular subtypes of urothelial carcinoma and gene signatures for molecular grading and outcome. Cancer Res 2010, 70:3463−3472
4. Sjödahl G, Lauss M, Lövgren K, Chebil G, Gudjonsson S, Veerla S, Patschan O, Aine M, Fernö M, Ringnér M, Månsson W, Liedberg F, Lindgren D, Höglund M: A molecular taxonomy for urothelial carcinoma. Clin Cancer Res 2012, 18:3377−3386
5. Jimenez RE, Gheiler E, Oskanian P, Tiguert R, Sakr W, Wood DP Jr, Pontes JE, Grignon DJ: Grading the invasive component of urothelial carcinoma of the bladder and its relationship with progression-free survival. Am J Surg Pathol 2000, 24:980−987
6. Amin MB: Histological variants of urothelial carcinoma: diagnostic, therapeutic and prognostic implications. Mod Pathol 2009, 22(Suppl 2):S96−S118
7. Nassar H, Sakr W: Variants of urothelial carcinoma. Pathology of the Urinary Bladder. Edited by Foster CS, Ross JS. Philadelphia, Saunders, 2004, pp 117−118
8. Cheng L, Montironi R, Davidson DD, Lopez-Beltran A: Staging and reporting of urothelial carcinoma of the urinary bladder. Mod Pathol 2009, 22(Suppl 2):S70−S95
9. Sing T, Sander O, Beerenwinkel N, Lengauer T: ROCR: visualizing classifier performance in R. Bioinformatics 2005, 21:3940−3941
10. Lauss M, Frigyesi A, Ryden T, Höglund M: Robust assignment of cancer subtypes from expression data using a uni-variate gene expression average as classifier. BMC Cancer 2010, 10:532
11. Lindgren D, Sjödahl G, Lauss M, Staaf J, Chebil G, Lövgren K, Gudjonsson S, Liedberg F, Patschan O, Månsson W, Fernö M, Höglund M: Integrated genomic and gene expression profiling identifies two major genomic circuits in urothelial carcinoma. PLoS One 2012, 7:e38863
12. He X, Marchionni L, Hansel DE, Yu W, Sood A, Yang J, Parmigiani G, Matsui W, Berman DM: Differentiation of a highly tumorigenic basal cell compartment in urothelial carcinoma. Stem Cells 2009, 27:1487−1495
13. Volkmer JP, Sahoo D, Chin RK, Ho PL, Tang C, Kurtova AV, Willingham SB, Pazhanisamy SK, Contreras-Trujillo H, Storm TA, Lotan Y, Beck AH, Chung BI, Alizadeh AA, Godoy G, Lerner SP, van de Rijn M, Shortliffe LD, Weissman IL, Chan KS: Three differentiation states risk-stratify bladder cancer into distinct subtypes [published correction appears in Proc Natl Acad Sci U S A 2012, 109:3600]. Proc Natl Acad Sci U S A 2012, 109:2078−2083
14. Chan KS, Espinosa I, Chao M, Wong D, Ailles L, Diehn M, Gill H, Presti J Jr, Chang HY, van de Rijn M, Shortliffe L, Weissman IL: Identification, molecular characterization, clinical prognosis, and therapeutic targeting of human bladder tumor-initiating cells. Proc Natl Acad Sci U S A 2009, 106:14016−14021
15. Bertucci F, Finetti P, Birnbaum D: Basal breast cancer: a complex and deadly molecular subtype. Curr Mol Med 2012, 12:96−110
16. Ho PL, Kurtova A, Chan KS: Normal and neoplastic urothelial stem cells: getting to the root of the problem. Nat Rev Urol 2012, 9:583−594
17. Rieger-Christ KM, Cain JW, Braasch JW, Dugan JM, Silverman ML, Bouyounes B, Libertino JA, Summerhayes IC: Expression of classic cadherins type I in urothelial neoplastic progression. Hum Pathol 2001, 32:18−23
18. Rebouissou S, Hérault A, Letouzé E, Neuzillet Y, Laplanche A, Ofualuka K, Maillé P, Leroy K, Riou A, Lepage ML, Vordos D, de la Taille A, Denoux Y, Sibony M, Guyon F, Lebret T, Benhamou S, Allory Y, Radvanyi F: CDKN2A homozygous deletion is associated with muscle invasion in FGFR3-mutated urothelial bladder carcinoma. J Pathol 2012, 227:315−324
19. Urist MJ, Di Como CJ, Lu ML, Charytonowicz E, Verbel D, Crum CP, Ince TA, McKeon FD, Cordon-Cardo C: Loss of p63 expression is associated with tumor progression in bladder cancer. Am J Pathol 2002, 161:1199−1206
20. Sørlie T, Perou CM, Tibshirani R, Aas T, Geisler S, Johnsen H, Hastie T, Eisen MB, van de Rijn M, Jeffrey SS, Thorsen T, Quist H, Matese JC, Brown PO, Botstein D, Lønning PE, Børresen-Dale AL: Gene expression patterns of breast carcinomas distinguish tumor subclasses with clinical implications. Proc Natl Acad Sci U S A 2001, 11:10869−10874
21. Blows FM, Driver KE, Schmidt MK, Broeks A, van Leeuwen FE, Wesseling J, et al: Subtyping of breast cancer by immunohistochemistry to investigate a relationship between subtype and short and long term survival: a collaborative analysis of data for 10,159 cases from 12 studies. PLoS Med 2010, 25:e1000279